

# Nanosecond pulsed discharges in distilled water-Part II: line emission and plasma propagation

A von Keudell , K Grosse  and V Schulz-von der Gathen 

Experimental Physics II-Reactive Plasmas, Ruhr-Universität Bochum, D-44780 Bochum, Germany

E-mail: [Katharina.Grosse@rub.de](mailto:Katharina.Grosse@rub.de)

Received 20 December 2019, revised 16 June 2020

Accepted for publication 10 July 2020

Published 27 August 2020



## Abstract

Nanosecond plasmas in liquids can initiate chemical processes that are exploited in the fields of water treatment, electrolysis or biomedical applications. The understanding of these chemical processes relies on unraveling the dynamics of the variation of pressures, temperatures and species densities during the different stages of plasma ignition and plasma propagation as well as the conversion of the liquid into the plasma state and the gas phase. This is analyzed by monitoring the emission of nanosecond pulsed plasmas that are generated by high voltages of 20 kV and pulse lengths of 10 ns applied to a tungsten tip with 50  $\mu\text{m}$  diameter immersed in water. The spectra are acquired with a temporal resolution of 2 ns and the emission pattern is modelled by a combination of black body radiation from the hot tungsten tip and the pronounced emission lines of the hydrogen Balmer series. The data indicate two contributions of the hydrogen line radiation that differ with respect to the degree of self-absorption. It is postulated that one contribution originates from a recombination region showing strong self absorption and one contribution from an ionization region showing very little self-absorption. The emission lines from the ionization region are evaluated assuming Stark broadening, that yielded electron densities up to  $5 \times 10^{25} \text{ m}^{-3}$ . The electron density evolution follows the same trend as the temporal evolution of the voltage applied to the tungsten tip. The propagation mechanism of the plasma is similar to that of a positive streamer in the gas phase, although in the liquid phase field effects such as electron transport by tunneling should play an important role.

Keywords: plasma in liquids, nanosecond plasma, optical emission spectroscopy

(Some figures may appear in colour only in the online journal)

## 1. Introduction

Discharges in water are widely used for wastewater treatment [1–4], plasma supported electrolysis [5, 6], or for biomedical applications [7]. A good overview can be found in the roadmap on plasma in liquids [8]. The in-liquid discharges are usually ignited in a pin-to-pin or pin-to-plate configuration [9] by

applying a high voltage (HV) pulse to an electrode. The temporal structure of this high voltage pulse determines significantly the physics of these discharges. If the pulse rise time is slow in the range of microseconds and very long pulses are used, Joule heating of the liquid and the formation of small bubbles with evaporated water occurs first before the Paschen criterion for ignition is met in the gas phase inside these bubbles. The plasma then expands these bubbles, a gaseous streamer channel is formed that propagates through the liquid and the water dissociation chemistry is triggered. These streamers might also branch and tree-like and/or bush-like emission patterns have been found depending on the powering of the electrode



Original content from this work may be used under the terms of the [Creative Commons Attribution 4.0 licence](https://creativecommons.org/licenses/by/4.0/). Any further distribution of this work must maintain attribution to the author(s) and the title of the work, journal citation and DOI.

[10, 11]. This very complex behaviour makes these microsecond plasmas in liquids a very complicated multi physics problem to describe. However, if the pulse rise time is of the order of only nanoseconds and the pulse length is limited also to only 10 ns of nanoseconds, the complexity of the discharge development is very much reduced. Due to the fast time scale, the inertia of the water adjacent to the pin electrode is so high, that any displacement and consecutive bubble formation is not possible. However, the nature of the creation of a plasma inside the liquid (and not in the gas in a bubble inside the liquid) on these short time scales is still an open question.

The plasma ignition mechanisms in nanosecond plasmas responsible for breakdown in liquids are widely debated and may significantly differ from discharge to discharge [12–18]: normally, the density in the liquid is so high that the creation of a typical electron avalanche that reaches electron energies sufficient for ionization is very unlikely due to the strong scattering of the electrons. Consequently, several ignition models assume the presence of regions of low density in the liquid in front of a high voltage electrode [19]. Such low density regions may be induced by Joule heating followed by local evaporation, liquid rupture due to high electric field gradients, the simple small displacement of the water layer adjacent to the electrode due to the electric field pressure, or the ignition in previously formed bubbles which are created at the tip of the powered electrode due to degassing [20]. The ignition models that are based on reaching the Townsend criterion inside a gaseous bubble or nanovoid in the liquid have to be distinguished from ignition models based on field effects. For example, the breakdown inside transformer oils has been described by the Zener theory based on the tunneling of electrons as the source of ionization during the propagation of a streamer inside a liquid in high electric fields [21, 22]. All these effects such as liquid rupture or the onset of electron tunneling depend on the microscopic nature of the development of such streamers and the details of the electric fields involved.

Recently, we analyzed such nanosecond plasmas in liquids and described the dynamic of bubble formation *after* plasma ignition using cavitation theory [23]. The energy balance of this cavitation bubble formation is related to the energy dissipated by the plasma at the moment of ignition. Good agreement between the measured dissipated power in the discharge and the dynamic of bubble formation has been found. The main fitting parameter of this model was the potential energy given by the product of the finite plasma volume times pressure at the end of the plasma pulse. Based on this model, it is, however, not possible to easily convert pressures and volumes into densities and temperatures of species inside the plasma. Therefore, a detailed spectroscopic study of the plasma itself at a temporal resolution of 2 ns is performed in this paper to gain more information about the plasma itself. The emission spectra are dominated by a broadband continuum and line emission from the hydrogen Balmer series. The origin of the continuum is discussed in the first part of this paper series and the line emission in this second part.

The analysis of the continuum in these spectra analyzed in the first part of this paper series [24] supports a strong contribution of black body radiation emitted by 10  $\mu\text{m}$  sized areas at the

hot tungsten tip. The tungsten electrode reaches quickly a typical temperature around 7000 K after plasma ignition, which is equivalent to the boiling temperature of tungsten at high partial pressures of tungsten. This temperature varies slightly during the plasma pulse. An additional spectral contribution of even higher temperature was attributed to a hot spot formation of even smaller dimensions at protrusions of the tungsten electrode. This contribution appears when the electron transfer at the solid liquid interface is very efficient. This is especially relevant at the beginning of the pulse, when field ionization of water molecules occurs and at the end of the pulse when field emission at the tungsten tip electrode may be present. After this hot spot formation, thermionic emission of electrons is expected to dominate. Plasma emission is the most intense at the rising and the falling edge of the plasma pulse, because the change in the electric fields causes a significant acceleration of electrons and thus a change in heating and plasma emission.

Besides the black body continuum, the Balmer series of hydrogen and the atomic oxygen line at 777 nm are visible with a pronounced temporal dependence during the plasma pulse. By a thorough analysis of these line emission patterns, we investigate the dynamics of the plasma propagating inside the liquid. By analysing the different broadening mechanisms of the hydrogen emission lines, information on the temporal variation of electron densities is derived. Based on the nature of the electronic processes leading to that emission, a consistent model is being developed for this peculiar type of plasma propagation.

## 2. Experiment

### 2.1. Experimental setup

Figure 1 shows a schematic of the experimental setup used for time-resolved optical emission spectroscopy of the nanosecond pulsed plasma. The HV pulses are generated by a pulse generator FPG 30-01NK10 (FID Technology GmbH). The pulses have a rising time of 2–3 ns and a pulse width of approximately 15 ns. A frequency of 15 Hz was applied as well as a voltage of 20 kV. The cable connecting the power supply and the plasma electrode is a 12 m long coaxial cable (RG213) with a back current shunt (BCS) mounted at a central position along the cable (with  $a = b = 6$  m in figure 1(a)). The BCS is used to measure the current flowing inside the coaxial cable which can be used for calculating the voltage pulse. A direct measurement of the current at the electrode tip is not possible due to electromagnetic interference inside the Faraday cage. Nevertheless, the current  $I$  can be estimated from the dissipated energy  $E$  that is derived from a comparison of the initial with the reflected pulses yielding  $E = 3$  mJ. If we assume a voltage pulse length of approx. 15 ns at a voltage amplitude of 20 kV, the current can be calculated from the energy yielding roughly  $I = 10$  A. The current density at the tungsten tip would be even more relevant for the analysis of the plasma since the current density may also vary locally due to the effects such as self-contraction being typical for high current density discharges. This is, however, not analyzed here, because it would be only based on the rough current estimates and better experiments would be required for any robust interpretation.

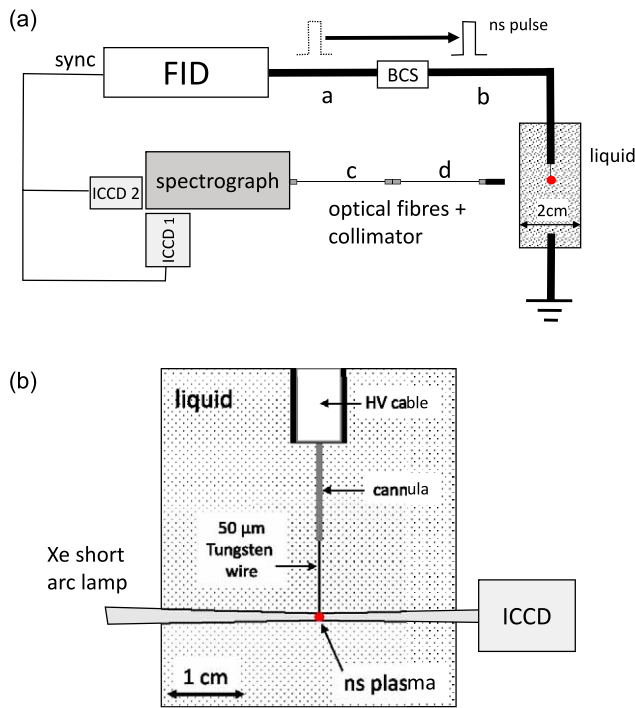


**Figure 1.** Sketch of the experimental setup showing the chamber from the side (a) and the front view of the chamber illustrating the electrode configuration and the ICCD imaging and Shadowgraphy setup in detail (b).

The electrical circuitry powering the nanosecond plasma can have a significant influence on the plasma by reflections and oscillations of the high voltage pulse inside the cable, if the plasma load is not matched to the impedance of the cable. The length of the cable connecting power supply and plasma electrode is a crucial parameter to distinguish between the forward and backward traveling pulses in the BCS signal. In the case of the 12 m long cable, the separation between the forward (initial) and backward (reflected) traveling pulse is approximately 60 ns and therefore, the voltage waveform at the electrode can unambiguously be determined. The difference between the initial and the reflected pulse can be used for determining the dissipated power and energy for a pulse of 15 ns which are in this case 200 kW and 3 mJ, respectively.

The electrodes are mounted into a PMMA made plasma chamber with three quartz windows for optical access (see figure 1(b)). They consist of copper rods insulated by glass tubes. Stainless steel cannulas are inserted in the copper rods to clamp a tungsten wire (diameter 50 μm) as electrode. Distilled water with an electrical conductivity of 1 μS cm<sup>-1</sup> and a pH of approximately 5.5 is used as the liquid. The plasma chamber and the FID pulser are both surrounded by a common Faraday cage so that electromagnetic interference (EMI) cannot escape the system.

For imaging and optical emission spectroscopy (OES) measurements an Andor iStar DH734-18U-03 camera is used. For OES the camera is mounted to a triple-grating SpectraPro 750 spectrograph from Acton Research, which used a 50  $\frac{\text{grooves}}{\text{mm}}$  grating, blazed at 600 nm. The system has an effective spectral resolution of about 2 nm. The camera is synchronized to

the discharge via the synchronization output of the FID pulser and a defined delay time to compensate for the cable length was set. The maximum jitter of the synchronisation signal is 0.5 ns and can, therefore, be neglected. By combining three spectra at different central wavelengths spectra of an overall wavelength range of approx. 600 nm could be recorded. Two connected UV suitable optical fibers from CeramOptec GmbH are used to couple the plasma emission into the spectrograph and to prevent EMI to escape from the Faraday cage. A collimator at the end of fiber *d*, which is mounted in front of the plasma chamber, collects the emitted light of the plasma into the optical system from a distance of about 4 cm. The 4 cm include a water layer of 1 cm from the electrode tip to the optical window. The system is calibrated with a broadband D<sub>2</sub>-Halogen lamp. The measurements are performed with a gate time of  $t_{\text{gate}} = 2$  ns and time steps of  $t_{\text{step}} = 2$  ns between the spectra within an interval of 30 ns. Each spectrum is averaged over 1000 discharges.

A more detailed description of the setup can be found in part I of this paper series [24].

## 2.2. Size of the plasma and sources of plasma emission

A single shot image taken of the plasma at 12 ns after ignition is shown in figure 2(a). In this phase, the plasma emission in the visible spectral range is the most intense. The image of the discharge shows that the maximum of emission is located in the direct vicinity of the electrode tip. Whereas the propagating plasma is only visible by faint structures developing up to the dotted circle. When the area of brightest emission is blackened, these structures become more visible, as discussed in the first part of this paper series (figure 13 in [24]). The diameter of the faint structures can be estimated roughly to be 100 μm from these images. Here it is important that the emission maximum is not located at the front of the propagating plasma (comparable to streamer head in gas discharges) but the location is close to the electrode tip. The good fit of black body radiation with temperatures of 6000–7000 K similar to the boiling temperature of tungsten led us to postulate that on the one hand black body radiation is the dominant source of the continuum radiation and that on the other hand the emitted black body radiation is likely to originate from the hot tungsten electrode [24].

Figure 2(b) shows a typical sketch of a plasma that propagates into the medium. In principle, one could start with the model of a positive streamer [25, 26]. However, the exact mechanism of plasma propagation in the very dense medium of a liquid may differ from the classical streamer in the gas phase, because recombination is more dominant and the mean free path of the electrons is reduced to inter molecular distances in liquid water. Therefore, we describe the nature of the propagating plasma in more general terms: the plasma is expected to propagate similar to a positive space charge region where a cloud of positive ions creates a high electric field in the surrounding that causes further ionization events. The newly created electrons are transported to the positive space charge where recombination occurs. In this simple picture the plasma structure should consist of a leading edge where ionization is dominant and a trailing part where recombination is

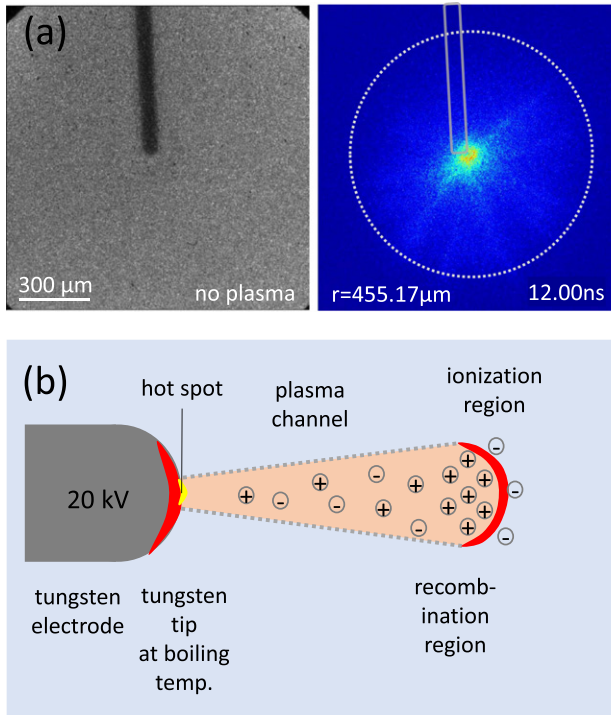


**Figure 2.** (a) Shadowgraphic image without plasma (left) and ICCD image of the discharge taken at 12 ns after ignition. The gray rectangular box indicates the position of the electrode. The gray circle with a radius of  $455\ \mu\text{m}$  describes the propagation distance of the streamers within the 12 ns. (b) Sketch of a plasma that propagates into the liquid starting from a hot spot on the tungsten electrode tip.

prevalent. When this plasma propagates through the liquid, a channel should be created along its path where the energy from the recombination events eventually leads to dissociation and heating of the water. This propagation of the plasma occurs with a velocity of approximately  $46\ \text{km s}^{-1}$  in our experiment [24], as described in part I of this paper series. Summarizing, we separate the propagating plasma into three regions: a leading *ionization region*, a trailing positive space charge region or *recombination region* and a *plasma channel* along the propagation path where dissociative recombination converts the liquid into hydrogen and OH.

With respect to light emission, we may postulate four contributions: (i) the black body emission from the tungsten tip at boiling temperature, (ii) black body emission from a hot spot at the tip of the tungsten electrode at the root of the plasma channel, (iii) light emission from a region where recombination dominates, (iv) light emission from a small region at the leading edge of the propagating plasma where the electron density is high and ionization dominates. The background of the spectrum is dominated by the contribution from black body radiation (i) and (ii), the line features in the spectra are dominated by the contributions from (iii) and (iv).

### 3. Spectral features

The emission spectra consist of a broad continuum and of broadened lines, as illustrated in figure 3 for a plasma

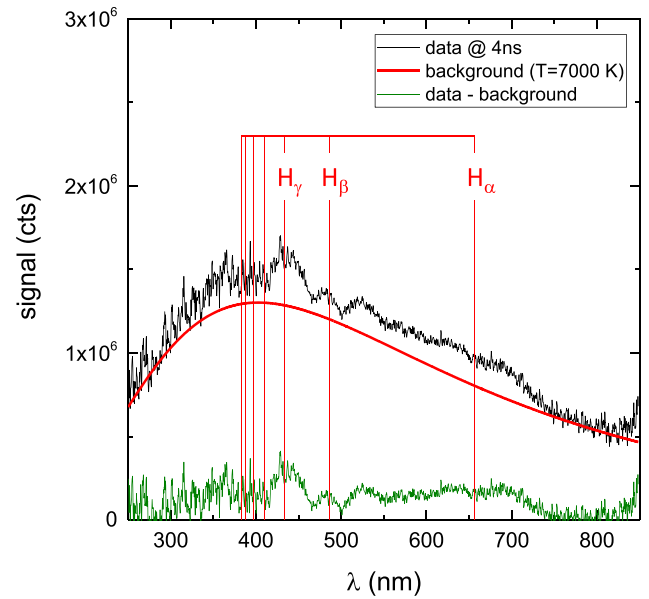


**Figure 3.** Emission spectrum at 4 ns after plasma ignition (black line). The line positions for hydrogen Balmer series are indicated.  $H_\alpha$ ,  $H_\beta$ , and  $H_\gamma$  are also labeled. The red line denotes a blackbody continuum for a temperature of 7000 K that is scaled to fit the data. After subtraction of this background the emission spectrum of the propagating plasma itself is plotted as green line.

measured at 4 ns after ignition. The red line corresponds to black body radiation assuming a temperature of 7000 K. This continuum spectrum is scaled arbitrarily to fit the data. After subtraction of the background, we obtain an emission spectrum that should only contain contributions from the propagating plasma itself (green line in figure 3).

The nature of the spectrum is consistent with the sketch of the propagating plasma and the single shot image of the plasma shown in figure 2. The spectrum is dominated by black body radiation from the tungsten tip, which is also the brightest spot in the single shot image. The line emissions contribute only to approximately 10% to the total number of generated photons. It is important to note that the image of the plasma above is a single shot image, whereas the spectrum is composed of 2000 discharges. The acquisition of spectra is performed using a quartz fibre that collects light from the complete region including electrode tip and propagating plasmas. Therefore, the light of all propagating plasmas in these 2000 discharges is properly collected despite the fact that the plasmas propagate in individual discharges in random directions.

#### 3.1. Continuum emission

In the first part of this paper series, we discussed the nature of the continuum. This continuum is dominated by black body radiation of the hot tungsten tip. Due to the high local current density an intense heating of tungsten occurs. This leads to typical black body temperatures of 7000 K or even higher. This temperature is consistent with the fact that the boiling temperature  $T_B$  of tungsten is at  $T_{B,p_0} = 5828\ \text{K}$  at ambient conditions corresponding to a vapour pressure  $p_0$ . During plasma



operation, non-negligible erosion of the tungsten tip occurs due to evaporation. This creates a higher tungsten vapour pressure in front of the electrode surface, that may cause the equilibrium surface temperature of the tungsten tip to increase even further. For example, if the partial pressure is increased by one or two orders of magnitude, the equilibrium temperature of a boiling tungsten surface may easily reach temperatures of 8000 K or higher.

Due to the local nature of the discharge, it is expected that this temperature is not homogeneously distributed over the surface of the tungsten tip, but a small hot spot on the hot tungsten surface may form, as it is known from arc lamp discharges [27], because the discharge current contracts the plasma to a particular location where the surface temperature is the hottest. Therefore, the overall black body radiation may be composed of the emission of the tungsten tip at boiling temperature plus a hot spot at even higher temperatures. The latter effect dominates, when the plasma current and the electron emission at the electrode is the highest. This occurs at the rising and the falling edge of the plasma pulse leading to an additional contribution to the broad band continuum at smaller wavelengths, as discussed in [24].

### 3.2. Line emission

In this paper, we regard the line emissions that become visible in the spectra. Since the plasma is ignited directly in distilled water, line emissions of only H and O containing atoms and molecules are expected. Any clear identification of emission lines is difficult, due to the very dynamic temporal evolution of the plasma, significant broadening effects and a limited signal-to-noise ratio at this high temporal resolution. Consequently, very many species may be formed during the dissociation of water, but a unique identification of, for example, OH emission with the prominent A-X bands at 306 nm is not possible. The only line emission that is clearly visible is the Balmer series of hydrogen, which is discussed in the following in detail.

Figure 3 shows the signature of spectral features at the line positions of the hydrogen Balmer series for  $H_\alpha$ ,  $H_\beta$  and  $H_\gamma$ . At later times after plasma ignition also a broadened oxygen emission line at 777 nm (OI(777 nm)) is observed. Due to the high temperatures and high densities of electrons and neutrals, all emission lines may be affected by Doppler broadening, van der Waals broadening or Stark broadening. The inspection of the spectra indicates full width at half maximum (FWHM) values of the lines of several nanometers at least, which is much larger than the Doppler broadening at temperatures of a few 1000 K. Therefore, only van der Waals and Stark broadening effects are discussed in the following. For these effects, the emission line should follow a line profile  $P(\lambda)$  of a Lorentzian for a central wavelength of  $\lambda_0$ :

$$P(\lambda) = \frac{1}{\pi} \frac{\left(\frac{\Delta}{2}\right)}{(\lambda - \lambda_0 - \lambda_s)^2 + \left(\frac{\Delta}{2}\right)^2} d\lambda \quad (1)$$

with  $\Delta$  the FWHM and  $\lambda_s$  a possible red shift of the line. The integration of the line profile yields  $\int P(\lambda) d\lambda = 1$ .

Other spectral features as e.g. emission from molecular components as e.g.  $H_2O$  or OH cannot be identified. The

limited spectral resolution combined with the signal noise and the broadening of the lines prohibit any unambiguous identification even of ro-vibrational bands.

### 3.3. Stark broadening

Stark broadening of emission lines in plasmas occurs due the perturbation of the emission process by electrons and ions surrounding the emitting atom or molecule. This broadening effect is quantified for the hydrogen Balmer series by Gigosos *et al* [28] in the form of tables of FWHMs for different temperatures and different reduced masses  $\mu$ . This reduced mass  $\mu$  describes the relation between the emitter atom hydrogen and the perturbing mass of the surrounding ions. Since, we assume that hydrogen emits and that the dominant ion is a water ion, we may use  $\mu \simeq 1$  amu. The value for the reduced mass can change in the case of non-equilibrium situations to  $\mu^* = \mu T_e / T_g$  for different electron and heavy particle temperatures. In the case of a high electron but low heavy species temperature, smaller Stark FWHM values [15, 29] compared to thermal equilibrium conditions are obtained.

According to the tables of Gigosos *et al*, the Stark effect at a temperature of 20 000 K and an electron density of  $10^{24} \text{ m}^{-3}$  yields an FWHM = 5 nm for the  $H_\alpha$  line, an FWHM = 23 nm for the  $H_\beta$  line, and an FWHM = 27.8 nm for the  $H_\gamma$  line. The  $H_\alpha$  FWHM varies typically by 5% for a temperature variation of a few 10 000 K, whereas the  $H_\beta$  and  $H_\gamma$  FWHM vary by 15% to 20%. Consequently, the  $H_\beta$  line is often used for Stark width analysis in plasma science since the line broadening is significant and the line is also sensitive to the plasma temperature [30]. The line width of  $H_\alpha$  is rather insensitive to temperature changes and simpler line width formulas consistent with the tables of Gigosos *et al* are available. One example are FWHMs  $\Delta_{H_\alpha}$  and red shifts  $\lambda_{s,\alpha}$  of the  $H_\alpha$  line as given by Kielkopf and Allard [31]:

$$\Delta_{H_\alpha} [\text{\AA}] = 1.55 \cdot 10^{-11} (n_e [\text{cm}^{-3}])^{0.70 \pm 0.03} \quad (2)$$

$$\lambda_{s,\alpha} [\text{\AA}] = 1.23 \cdot 10^{-16} (n_e [\text{cm}^{-3}])^{0.92 \pm 0.03} \quad (3)$$

The estimates are only validated up to electron densities of  $10^{25} \text{ m}^{-3}$  and any application at higher electron densities is an extrapolation. The red shift of the lines due to the Stark effect is usually rather small and typically only 10% of the FWHM.

In the extreme nanosecond plasmas in liquids, the visibility of lines and their separation from the background of the spectrum makes the identification of lines and their FWHM and shift very challenging. For example, a broadened hydrogen  $H_\alpha$  line is clearly visible in the spectra with an FWHM of typically of 80 nm, as shown below. Since the center of the line is shifted by 10% of the FWHM, the Stark effect is identified as the line broadening mechanism. Consequently, one would expect to also observe Stark broadened  $H_\beta$  and  $H_\gamma$  lines. The line intensities of  $H_\beta$  and  $H_\gamma$ , however, are one or two order of magnitudes smaller due to the lower population of the upper states and the much lower transition probabilities of  $H_\beta$  and  $H_\gamma$  in comparison to  $H_\alpha$  (Einstein coefficients for spontaneous emission are  $A_{H_\alpha} = 4.41 \times 10^7 \text{ s}^{-1}$ ,  $A_{H_\beta} = 8.419 \times 10^6 \text{ s}^{-1}$ , and  $A_{H_\gamma} = 2.53 \cdot 10^6 \text{ s}^{-1}$ , respectively). Consequently, if one

observes a Stark broadened  $H_\alpha$  line with an FWHM of 80 nm, an order of magnitude smaller  $H_\beta$  or  $H_\gamma$  line with a typically 4 times larger FWHM compared to the FWHM of  $H_\alpha$  cannot easily be distinguished from the background continuum.

### 3.4. van der Waals broadening

The second broadening mechanism that influences the FWHM of the hydrogen Balmer series is likely van der Waals broadening that is induced by collisions of hydrogen with surrounding collision partners. The van der Waals broadening is extracted from the formulas of Konjevic *et al* [32] yielding an FWHM:

$$w[\text{cm}] = 8.18 \times 10^{-12} \lambda^2 [\text{cm}^2] (\alpha [\text{cm}^2] R^2)^{2/5} \times (T[\text{K}] / \mu [\text{amu}])^{3/10} n [\text{cm}^{-3}] \quad (4)$$

with  $\lambda$  the wavelength of the emission in [cm],  $\alpha$  the polarizability of the collision partners [ $\text{cm}^2$ ],  $T$  the temperature of the gas [K], and  $\mu$  the reduced mass describing the collision of hydrogen and the collision partners [amu]. The factor  $R^2$  can be extracted from the quantum numbers of the transition by  $R^2 = R_u^2 - R_l^2$  with

$$R_u^2 = 0.5n_u^2(5n_u^2 + 1 - 3l_u(l_u + 1)) \quad (5)$$

$$R_l^2 = 0.5n_l^2(5n_l^2 + 1 - 3l_l(l_l + 1)) \quad (6)$$

with  $n_u$ ,  $n_l$  the main quantum numbers of the upper and lower state of the transition.  $l_u$ ,  $l_l$  are the angular momentum quantum numbers of the upper and lower states. The polarizability  $\alpha$  may range from  $1.45 \times 10^{-18} \text{ m}^2$  for water to  $0.8 \times 10^{-18} \text{ m}^2$  for oxygen or  $0.66 \times 10^{-18} \text{ m}^2$  for hydrogen as collision partners. If we assume that van der Waals broadening of hydrogen atoms is induced by collisions with water molecules at a density of  $3 \times 10^{28} \text{ m}^{-3}$  corresponding to the liquid density of water. Previously, we analyzed the pressures during plasma evolution and expansion by a modelling based on cavitation theory [23]. This yielded a gas density of liquid water and a temperature of a few thousand K during the plasma phase at the very beginning. If we use the very same estimate to assess the van der Waals broadening, one would expect FWHMs of 65 nm for  $H_\alpha$ , of 34 nm for  $H_\beta$  and of 26 nm for  $H_\gamma$ . These high values should correspond to an upper limit. It is reasonable to assume that collision partners consist of hydrogen or oxygen atoms with much smaller polarizabilities and that the local densities at the location of the emitting atoms can be somewhat smaller than the liquid water density. If we assume for example hydrogen as emitter inside water at a reduced density of  $3 \times 10^{27} \text{ m}^{-3}$  and a temperature of 7000 K, one obtains FWHM values of 6.5 nm for  $H_\alpha$ , 3.4 nm for  $H_\beta$  and 2.6 nm for  $H_\gamma$ . An FWHM of up to 80 nm, as visible for the  $H_\alpha$  line in the spectra could only be explained by water molecules as collision partners at a density of liquid water of  $3 \times 10^{28} \text{ m}^{-3}$  and a temperature of 15 000 K. This seems unrealistic.

The van der Waals effect causes also a shift to the red of 33% of the FWHM [33], which is much larger than the shift of 10% of the FWHM due to the Stark broadening. Therefore, the nature of the broadening mechanisms for very broad lines can easily be identified by regarding both, the FWHM and the

shift of the line. For example, the  $H_\alpha$  line with an FWHM of 80 nm that is observed in the data at 14 ns after plasma ignition is shifted by 8 nm only, consistent with the Stark effect being the line broadening mechanism. Therefore, we assume that the impact of van der Waals broadening is much smaller in comparison to the line broadening by the Stark effect for very large FWHM values.

### 3.5. Self absorption

The high density of species in the nanosecond plasma, causes also self absorption of the emission lines [34, 35] and can be seen in the spectrum shown in figure 3 as small line reversal of the  $H_\alpha$  line. Self absorption of an emission line takes into account that the emitted photons of a transition may be reabsorbed by the very same species along the optical path. This effect can be calculated by using an optical depth  $p$  given by:

$$p = \frac{h\nu_0}{c} B P(\lambda_0) \int n_a(x) dx \quad (7)$$

with  $h$  Planck's constant,  $\nu_0$  the frequency of the emission line,  $B$  the Einstein coefficient of absorption and  $P$  the line profile. The integral  $\int n_a(x) dx = N_a$  yields the total number of absorber species  $N_a$  along the optical path. The Einstein coefficient  $B$  for absorption is connected to the Einstein coefficient for spontaneous emission  $A$  via:

$$A = \frac{2h\nu^3}{c^2} B = \frac{2hc}{\lambda^3} B \quad (8)$$

with  $c$  the velocity of light. This yields a modification of an emission line  $I(\lambda)$  with a line profile  $P(\lambda)$  and amplitude  $I_0$  passing a layer with absorbing atoms of the same identity of [34]:

$$I(\lambda) = I_0 P(\lambda) \exp \left( -p \frac{P(\lambda)}{P(\lambda_0)} \right) \quad (9)$$

This is the simplest case of a spatial separation of emitters and absorbers. Since the nanosecond plasma is very much localized, we assume that this situation describes our case and the hydrogen emitting at the center of the plasma in the recombination region or in the ionization region are affected by dissociated cloud of hydrogen atoms in the surrounding.

Self absorption of emission lines mainly affects the center of a line and leads to a peculiar change of the line shape. This needs to be distinguished from a regular absorbing medium, which influences the overall line intensity but not the line shape. The absorption coefficient of liquid water in the wavelength region of the Balmer series is very small of the order of  $10^{-4}$  to  $10^{-2} \text{ cm}^{-1}$  and can be neglected. More important is the influence of the optical path  $x$ . Along this path, a significant density of the lower states of the transition of the emitting species needs to be present for the self-absorption effect to become visible. In case of the hydrogen Balmer series, this constitutes to the  $n = 2$  state of hydrogen. Such states are excited states of hydrogen and should only be dominant in the plasma filaments, either at the leading edge or in the recombination region behind the streamer head. From the inspection of the ICCD image above, we estimate that such optical lengths are in the range of 100  $\mu\text{m}$  at most.

## 4. Results

To understand and discuss the dynamics of the line emission, the temporal evolution of the emission spectrum has to be correlated with the applied voltage. In part I of this paper this was performed with a focus on the continuous emission.

### 4.1. Voltage characteristics and emission from the plasma

The temporal evolution of the initial and reflected BCS voltage and of the electrode voltage are shown in figures 4(a) and (b), respectively. Additionally, figure 4(b) shows the integrated light from the camera images. One can clearly see two intensity maxima in the emission which are correlated to the rising and falling edge of the high voltage pulse. In between, a dark phase of the pulse, as already reported in the literature [19, 36], can be identified. The synchronization of electrical and optical signals can also be performed by correlating the voltage plateau and the dark phase in emission. A direct synchronization between optical and electrical signals could not be realized for the present measurements. In the first part of this paper series, we connected these emission maxima with the ignition phenomenon at the beginning of the pulse corresponding to field ionization of water molecules at small protrusions at the tungsten electrode tip. This instantaneous formation of positive ions in proximity of the tungsten electrode leads to the seed ions for the plasma to propagate following a mechanism similar to a streamer mechanism in the gas phase, as discussed below. These fast ionization processes may induce light emission due the acceleration of the electrons in the high local fields inducing that emission maximum. At the end of the pulse, the voltage is being switched off and an electric field acts on the plasma channel, leading to an acceleration of residual electrons and to field emission at small protrusions at the tungsten electrode tip. A second maximum in emission becomes visible as shown in figure 4. The postulated temporal correlation of the voltage evolution and emission intensity needs to be validated in future experiments by an accurate synchronization of both signals. Nevertheless, these processes describe the discharge behaviour and evolution inside the liquid reasonably well under the assumption that the correlation between intensity and voltage is given.

The voltage measured at the BCS and the acquisition by the camera and by the emission spectrometer are synchronized, but the absolute time delay between these data sets is difficult to calibrate. Instead, we used the most characteristic point in the data at the end of the plasma pulse at the maximum of the voltage, to shift the voltage curves, the camera images and the emission spectra by a few nanoseconds to fix a common unique time axis. Such a shift may seem arbitrary, because delays between voltage and emission are well known to occur for gaseous streamers and ionization avalanches [37]. But, as it is known from literature [14], the plateau of the voltage pulse is equivalent to the time of lowest intensity and therefore this assumption is taken for shifting both axes.

The corresponding emission spectra taken at high temporal resolution are shown in figure 5 (same data as in part I of the series). The individual spectra are stacked in the graph

and scaled for best visibility of the spectral features. One can clearly see a pronounced and very broad  $H_\alpha$  peak, especially at later times after plasma ignition. Complex spectral features at the location of the  $H_\beta$  and  $H_\gamma$  lines are also clearly visible. At later times, a broadened line at the position of  $OI(777\text{ nm})$  also appears. The temporal development of the spectra indicates that the Balmer lines are not much shifted with respect to the standard line positions. This indicates that Stark broadening appears to be the dominant broadening mechanism at least for the broad  $H_\alpha$  line.

### 4.2. Separating line emission from background emission

The analysis of the line emissions in the spectra requires first the subtraction of the background and then the fitting of the emission lines of the Balmer series. At first, the black body radiation from the hot tungsten tip including the possible formation of a small hot spot at the foot print of the plasma, as discussed in part I of this paper series is modelled. Then, the background subtracted spectra are fitted using an emission model for the hydrogen Balmer series. The best fit is obtained, if two main contributions are being postulated for hydrogen Balmer line emission:

- *Balmer series emission from hydrogen atoms in the ionization region:* the ionization region is the location of high electron densities and it is reasonable to assume that Stark broadening dominates line emission of the hydrogen lines from this location. The leading edge of the propagating plasma, where the electric field is expected to be the highest is also a very small region in comparison to the complete plasma channel, so that self absorption of the lines should play only a minor role.

In addition, excitation of hydrogen by fast electrons that are accelerated in the electric field around the leading edge of the propagating plasma should be the dominant process. This should lead to a population of excited states of hydrogen that can be described by an electron temperature. In this case, the line emission from  $H_\alpha$  in the Balmer series will dominate.

- *Balmer series emission from hydrogen atoms in the recombination region:* the recombination region behind the ionization region of the propagating plasma exhibits lower electron densities and Stark broadening effects might be similar to van der Waals broadening in this region. In addition, the recombination region represents almost the complete volume of the propagating discharge so that any self absorption effects may influence the emission line shapes much stronger than for the emission from the ionization region.

In a recombination reaction of a proton and an electron, higher states of hydrogen are populated first inducing light emission from cascade processes. In this case, strong deviations from a thermal population of the excited states of hydrogen are expected. For example, if recombination leads to the population of the  $n = 5$  state in hydrogen first, the line emission of  $H_\gamma$  in the Balmer series will be enhanced. In general, the differences in energies of the

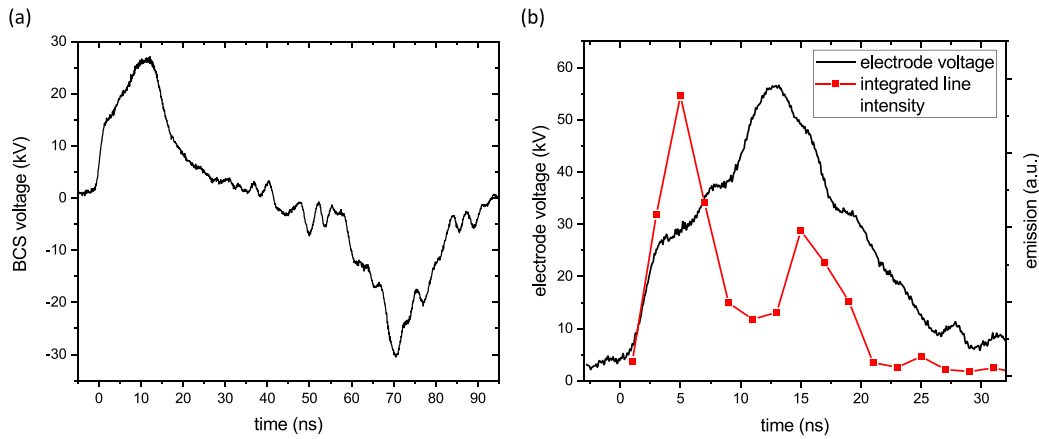


**Figure 4.** Temporal evolution of the (a) BCS voltage, (b) the electrode voltage (black line) and the integrated light emission acquired by the camera (red solid symbols).

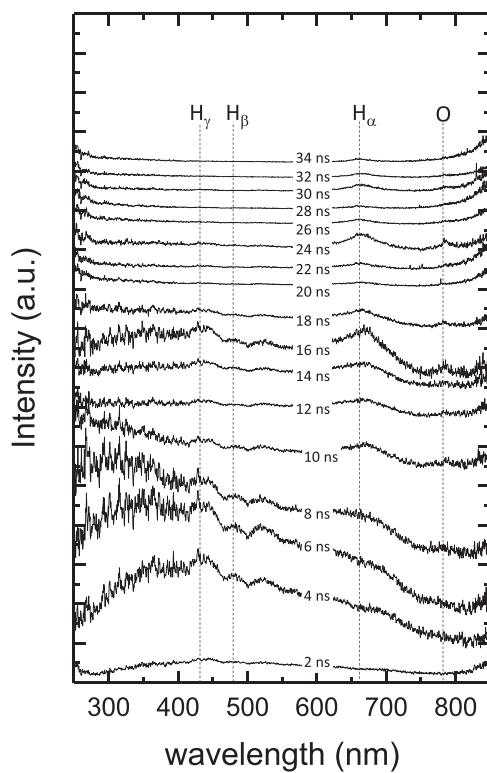


**Figure 5.** Time-resolved emission spectra of the discharge arising after ignition. The line positions for hydrogen Balmer series and for the OI(777 nm) emission are indicated.

$n = 3$ ,  $n = 4$ , and  $n = 5$  states in hydrogen are only  $\approx 1$  eV. At an estimated temperature of 7000 K, the differences in population are therefore only a factor 5 at most assuming a Boltzmann equilibrium, but not orders of magnitude.

This separation in two regions of origin of the hydrogen Balmer series generates a typical spectrum, where the emission from the ionization region is dominated by a Stark broadened  $H_\alpha$  line with  $H_\beta$  and  $H_\gamma$  being barely visible, because these lines are much smaller, but also much broader due to

their higher sensitivity to the Stark effect. This is in contrast to the emission from the recombination region, where  $H_\beta$  and  $H_\gamma$  radiation from recombination dominates and the much stronger  $H_\alpha$  emission is reduced due a strong self absorption effect. Using this simple model of two hydrogen emission populations, the background corrected spectra can be very well fitted as shown in figure 6.

Figures 6(a)–(e) show the data at different times after plasma ignition and the corresponding modelling of the continuum background consisting of black body radiation assuming a temperature between 5200 K and 7900 K as indicated and a second contribution of black body radiation at a very much higher temperature. Details of this are discussed in part I of this paper series. Figures 6(a')–(e') show the residuum (signal-background) on a same scale. It can be noted that the residuum exhibits a deviation from zero especially at wavelengths above 750 nm and also below 280 nm, which is especially pronounced when the absolute signal intensity is small as can be judged from the different scales in figures 6(a)–(e). These deviations are an artifact from the calibration procedure and originate from the subtraction of the background light from the data. This induces significant error in the wavelength region where the detection system exhibits a poor sensitivity as it is the case below 280 nm and above 750 nm.

This fit is based on the parameters amplitude and FWHM for each Balmer line originating either from the recombination or from the ionization region. In addition, a total number of absorbers is used to describe the self absorption for the complete Balmer emission for each of the regions. The black body background is described by a temperature and an amplitude. This yields 10 free parameters for this fitting. Such a large number of fitting parameters can render a model ambiguous, but different parameters are affecting very different parts of the spectra and different features of the Balmer series that can easily be separated from the continuum background. The most robust parameters are the FWHM and amplitude of the  $H_\alpha$  line originating from the ionization region and the corresponding number of absorber atoms. The emission lines from the recombination region suffer all from strong self absorption,



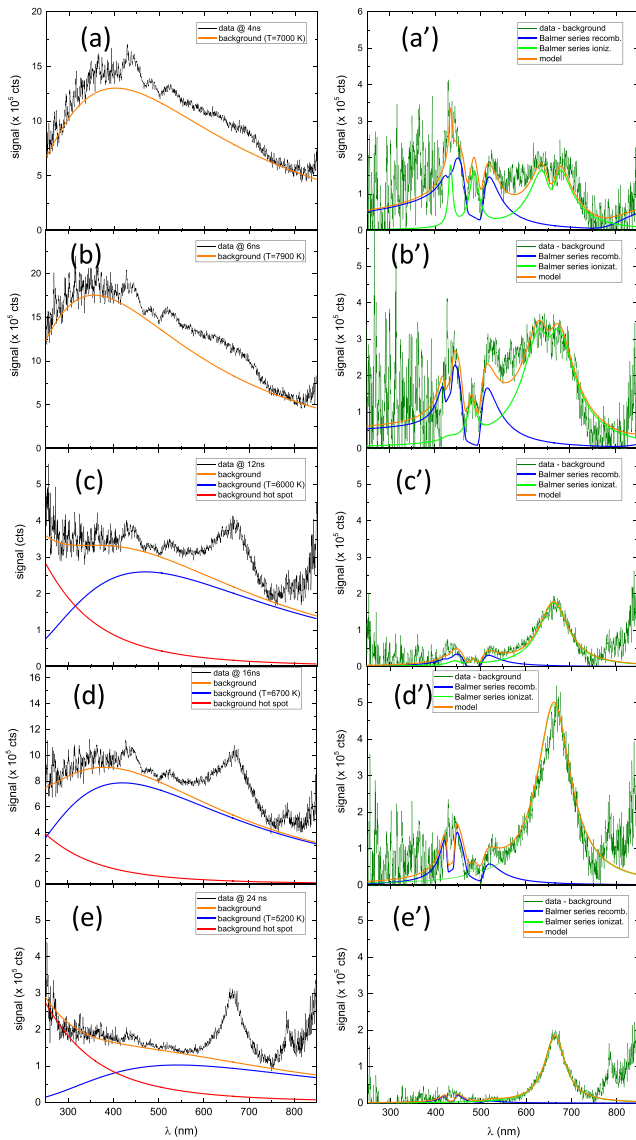


**Figure 6.** (a)–(e) Fitting of the original spectrum (black line) with a continuum background (orange line) that is composed of black body radiation from two contributions described by an overall temperature between 5200 K and 7900 K, as indicated (blue line), and the emission of a small hot spot at 20 000 K (red line); (a')–(e') fitting of the residuum of data minus background (green line). The data correspond to times after ignition of 4 ns (a, a'), 6 ns (b, b') during build up of the streamer, 12 ns (c, c') during the dark phase, 16 ns (d, d') at switch off of the voltage and the start of the falling voltage slope, and 24 ns (e, e') during the decay of the plasma. The modelled emission spectrum of the plasma (orange line) consist of contributions of the hydrogen Balmer series originating from the recombination region (blue line) and from the ionization region (green line). Emission from the ionization and recombination region differ with respect to self absorption.

which makes the fitting of the amplitude, of the FWHM, and of the absorber numbers much less reliable. The error bars for these fitting parameters express the ambiguity in their absolute values. The amplitudes of the lines depend very much on the excitation process, but also on the volume of the emission region. This will be discussed below. At first, we discuss the line shapes in the spectra in figure 6 as follows:

- *at 4 ns after ignition (figure 6(a))*: the  $H_{\alpha}$  line originating from the ionization region shows a small degree of self absorption indicating the existence of absorbing hydrogen atoms in the optical path at the very beginning of the discharge. The  $H_{\beta}$  and  $H_{\gamma}$  line show strong self absorption line shapes. At the central position of the  $H_{\beta}$  and  $H_{\gamma}$  line, a broadened line without any self absorption is still visible. Such a contribution indicates hydrogen emission in the absence of self absorption. These emitting hydrogen atoms cannot originate from the ionization region, because the FWHM should be much larger than the FWHM of the  $H_{\alpha}$  line from the very same region. Instead, these small  $H_{\beta}$  and  $H_{\gamma}$  contributions may originate from a separate region of hydrogen atom emission outside of the central part of the propagating plasma. This is just a hypothesis and further experiments would be required to uniquely identify this small contribution.
- *at 6 ns after ignition (figure 6(b))*: the amplitude of the  $H_{\alpha}$  line is increasing and the line shows less self absorption. The FWHM is also larger indicating a larger electron density. This trend can be easily understood. At the beginning of the discharge, more and more hydrogen atoms are being ionized, which causes an increase in electron density, but at the same time a decrease in hydrogen absorbers inducing self absorption. The plasma propagation apparently outruns the formation of neutral hydrogen atoms due to field effects in the vicinity of the electrode.
- *at 12 ns after ignition (figure 6(c))*: the FWHM of the  $H_{\alpha}$  line is very large and shifted typically by 10% of the FWHM indicating the Stark effect being the broadening mechanism. At the same time, the emission pattern of the  $H_{\beta}$  and  $H_{\gamma}$  line remains unaltered, but their contribution in relation to the  $H_{\alpha}$  line becomes smaller. At later stages in the plasma propagation, the density along the plasma channel might decrease and the electron temperature cools down, so that the hydrogen emission from this region becomes fainter as the plasma propagates.
- *at 16 ns after ignition (figure 6(d))*: the  $H_{\alpha}$  line shape is very similar to the spectrum at 12 ns. The typical slight asymmetry to the red of the Stark broadened line becomes visible. A broad line for the OI(777 nm) emission appears at 777 nm.
- *at 24 ns after ignition (figure 6(e))*: the  $H_{\alpha}$  line is dominant in the spectrum with a smaller FWHM indicating lower electron densities. The spectral signatures of the  $H_{\beta}$  and  $H_{\gamma}$  line become weaker indicating that during the decay of the plasma, the electron temperature in the plasma channel may decrease causing the lines to become rather faint very quickly.

The good agreement between data and emission model assuming two major contributions of emitting hydrogen atoms yields line parameters for the  $H_{\alpha}$ ,  $H_{\beta}$ , and  $H_{\gamma}$  lines for the ionization regions and the recombination region and two numbers of absorbing species. The parameters line amplitude, FWHM and number of absorbers causing self absorption are coupled and lead to a certain ambiguity in the absolute values. The most robust parameters are the absorber numbers and the line

parameters for the pronounced  $H_\alpha$  line of the emission from the ionization region. The detailed fitted parameters of the  $H_\beta$  and  $H_\gamma$  lines are discussed only to a small extent in the following, because they may suffer from larger error bars and also from the effect that the recombination region may be composed of different spatially separated parts. Here, the simple model of a unique distribution of hydrogen atoms may be an oversimplification.

A good fit is obtained by assuming a number density of  $N_a = 4 \times 10^{16}$  absorber atoms along the optical path for the hydrogen atoms emitting in the recombination region. The plasma propagates in random directions from the tungsten electrode, so that most of the light emission from the recombination region escapes along the sides of the plasma channel. If we assume an optical path length of photons escaping from this channel of typically  $100 \mu\text{m}$ , one may deduce a density of absorbing hydrogen atoms of  $n_a = 4 \times 10^{20} \text{ m}^{-3}$ . The  $n = 2$  state of hydrogen is  $10.2 \text{ eV}$  above the ground state. If we assume the black body temperature of the tungsten tip of typically  $7000 \text{ K}$  being also representative for the gas temperature in the recombination region, we can derive a ground state density of  $n_0 = n_a \exp(10.2 \text{ eV}/7000 \text{ K})$  of  $8.8 \times 10^{27} \text{ m}^{-3}$ . This is close to the liquid density of water and leads to the conclusion that water may be completely dissociated within the recombination region, producing a very high local density of hydrogen atoms. This complete dissociation of water in the recombination region is consistent with chemical kinetics calculations of the water chemistry in the nanosecond plasma [38].

An absorber number  $N_a$  of only a few  $10^{13}$  absorber atoms along the optical path for the hydrogen atoms emitting from the ionization region is necessary to fit the data. This much smaller number may be compared to the estimate for the self absorption in the recombination region: when an absorber number  $N_a$  of  $10^{16}$  corresponds to a length scale of  $100 \mu\text{m}$  in the recombination region, an absorber number of  $10^{13}$  should correspond to an optical path for self absorption of light from the ionization region of the order of  $1 \mu\text{m}$  or even below. This is consistent with typical models for propagating plasmas in the literature such as streamers. As a streamer propagates, only at the very tip a high electric field is created that accelerates electrons into the streamer head. If we transfer this typical picture of streamer discharges to the in liquid discharge, excitation and emission would occur in a very thin layer of around  $1 \mu\text{m}$  at the head of the filament.

#### 4.3. Electron densities and dynamic of the nanosecond plasma

The line profiles of the  $H_\alpha$  line originating from the ionization region are fitted assuming Stark broadening including the effect of self absorption. The electron densities are then derived from the FWHM using equation (2). The temporal evolution of the electron density is shown in figure 7(a) together with the temporal evolution of the voltage for comparison. The electron density reaches very high values of the order of  $5 \times 10^{25} \text{ m}^{-3}$  at the end of the pulse (this implies the validity of the extrapolation of equation (2) to electron densities slightly above  $10^{25} \text{ m}^{-3}$ ). These data are consistent with our previous experiment [23], as shown in figure 7(b) comparing the new

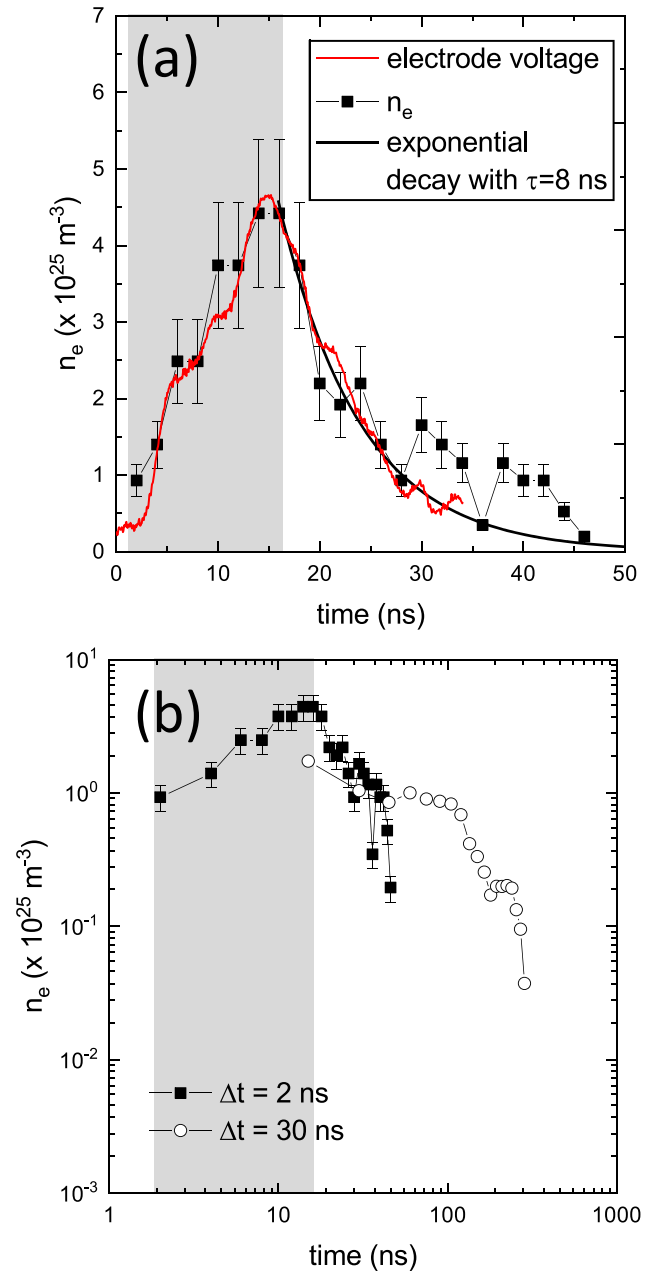


**Figure 7.** Electron densities as extracted from the FWHM of the  $H_\alpha$  line. The red line denotes the temporal evolution of the electrode voltage for comparison. (a) Comparison of the temporal evolution of the electron density  $n_e$  with the voltage, the exponential decay is modelled by a solid line using a decay constant of  $8 \text{ ns}$ . The gray area indicates the rising part of the voltage. (b) Electron densities in this work (solid symbols) compared with the data from a previous publication (8.65 m cable) using a temporal resolution of  $30 \text{ ns}$  [23].

data taken at a temporal resolution of  $2 \text{ ns}$  with the previous data taken at a temporal resolution of  $30 \text{ ns}$ . Such electron densities are typical for discharges in liquids for a wide range of pulse lengths [8, 9, 39].

It is striking that the electron density follows closely the voltage applied to the electrode during the rising and falling edge of the pulse. In nanosecond plasmas in gases at atmospheric pressures, the voltage and current exhibit usually a delay in between with the voltage rising first followed by the

current due to the delayed build-up of the electron density in the ionization avalanche. During the plasma propagation in the liquid, however, the density of species is three orders of magnitudes higher, so that the build-up of charges is expected to be much faster compared to the variation of the voltage. The same also holds for recombination that should exhibit time constants of the order of ps at these densities. The actual electron density is then a balance between generation of free electrons in the high electric fields and their loss due to recombination. This is consistent with the observation that the electron density follows also the decrease of the voltage with a time constant of 8 ns (shown as solid line in figure 7(a)). The decay of the electron density is not a free decay due to recombination, but rather follows a decreasing equilibrium value as a competition between ionization and recombination.

A close inspection of the data indicates also an oscillation of the electron density during the decay with a period of  $10^{-8}$  s. This is similar to the time constant of the nanosecond pulse itself. Any further interpretation of the temporal evolution of the electron densities at 20 ns after plasma ignition and later remains ambiguous, because the effects of van der Waals broadening on the FWHM cannot easily be distinguished from the Stark broadening at electron densities below  $10^{25} \text{ m}^{-3}$  in our high pressure nanosecond plasmas.

The interpretation of the  $H_\alpha$  line width using the Stark effect may be questionable taking into account that pressure broadening might also be significant given the very high pressures in our plasmas. However, Stark broadening and pressure broadening can be distinguished based on the shift of the lines, which is only 10% in case of Stark broadening but 30% of the wavelength in case of pressure broadening. In our experiment we see only a shift of 10%. Therefore, we assume that Stark broadening is dominant and that the shift of the  $H_\alpha$  line and its width can be directly connected to an electron density.

In the following, we discuss the line parameters of the most prominent  $H_\alpha$  emission originating from the ionization region. Figure 8 shows the temporal evolution of the number of absorbers  $N_a$  (a), the amplitude of the  $H_\alpha$  line (b), and the temperature of the hot tungsten tip (c) for comparison. The temporal evolution of the voltage and of the electron density, as shown in figure 7, are also plotted as reference.

The number of absorbers is of the order  $N_a = 3 \times 10^{13}$  at the very beginning of the discharge (figure 8(a)). It decays to zero at 10 ns simultaneously with the increase in electron density. This behaviour can easily be explained. At the beginning of the discharge, field ionization creates the first positive ions in the vicinity of the tungsten tip. This positive space charge starts to propagate and causes dissociation and excitation of water molecules and their dissociation products. As the plasma propagates more and more hydrogen atoms are converted into hydrogen ions and are thereby not able to act as absorber atoms anymore or the total numbers of hydrogen atoms in front of the propagating plasma becomes so small that any self absorption cannot longer be identified in the line profiles.

The amplitude of the  $H_\alpha$  emission from the ionization region is a measure of the volume or the size of the plasma that is propagating (figure 8(b)). At the beginning of the discharge, the amplitude is rather large, whereas the electron density is

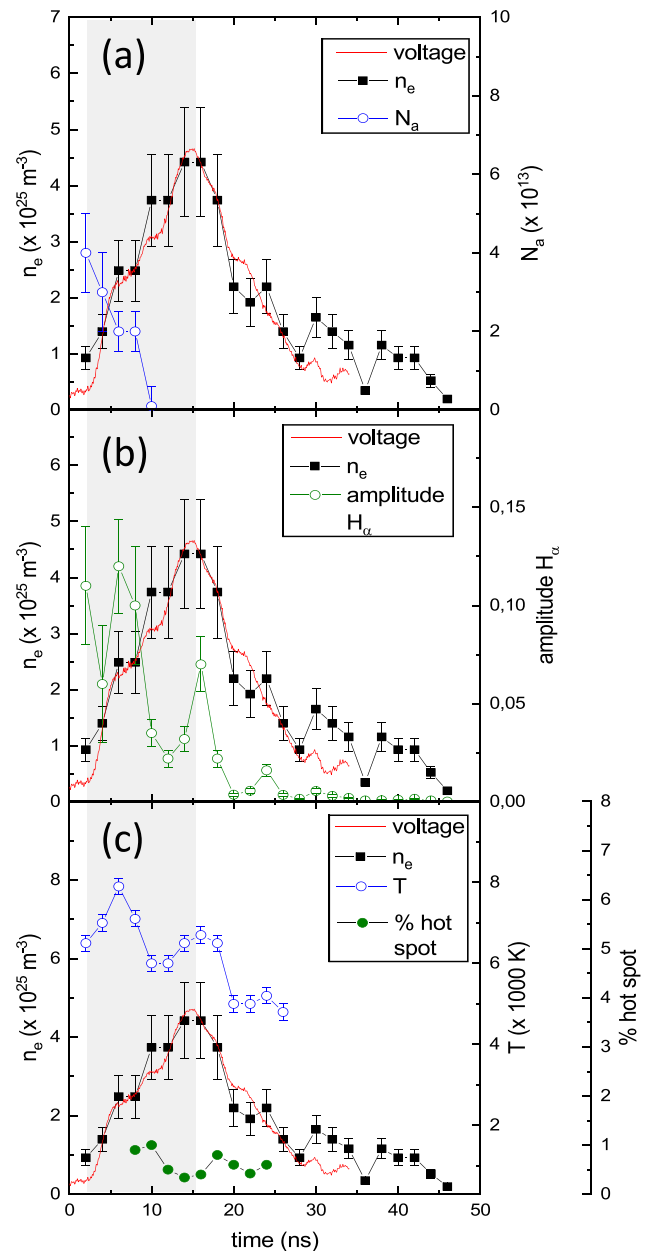


**Figure 8.** Temporal evolution of the fitted line parameters of the  $H_\alpha$  line. The temporal evolution of the electrode voltage is shown as a red line. (a) Change of the number  $N_a$  of absorbers along the optical path, (b) amplitude of the  $H_\alpha$  line, (c) variation of the black body continuum expressed as temperature and the percentage of the contribution of a hot spot at 20 000 K. The gray area indicates the time of the plasma pulse.

still small. This is consistent with a distribution of emitting hydrogen atoms over a large area in the vicinity of the tungsten surface, where field effects cause ionization and excitation. As time progresses, the amplitude decreases sharply and the electron density increases. This can correspond to a localization of the plasma at the electrode tip and may resemble a typical dynamic of the formation of an arc spot. This is in line, with the observed variation of the radiation from the tungsten tip: simultaneously with a localization of the  $H_\alpha$  emission, the black body temperature of the tungsten tip decrease

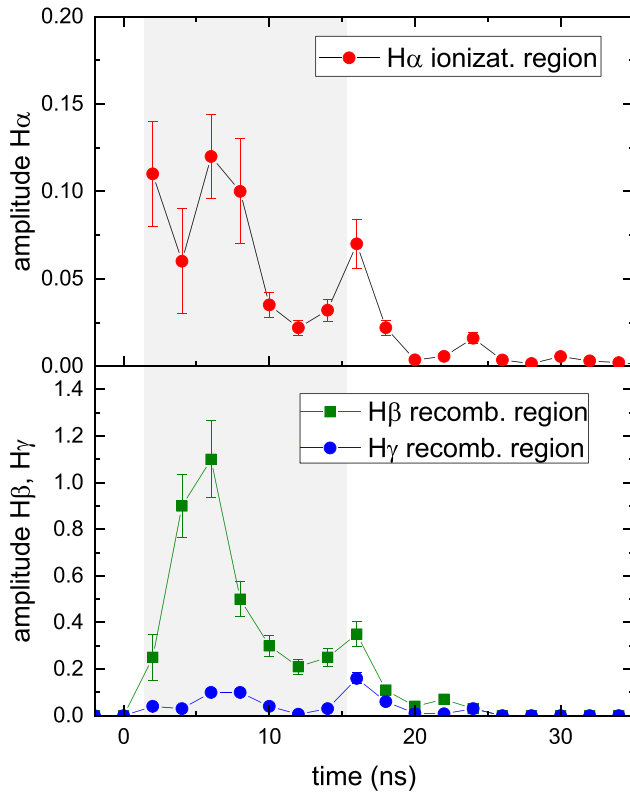


**Figure 9.** Amplitude of the H $\alpha$  line emitted from the ionization region (a). Amplitude of the H $\beta$  and H $\gamma$  line emitted from the recombination region. The gray area indicates the rising part of the voltage.

whereas the contribution from a hot spot causing a shift of the continuum to shorter wavelengths becomes visible, as can be deduced from the fitting parameters of the black body continuum shown in figure 8(c). At the location of the hot spot, tungsten is efficiently evaporated inducing evaporation cooling leading to a lowering of the temperature in the region surrounding this hot spot. At the end of the pulse, the amplitude of the H $\alpha$  line goes through a short maximum, because the change in the electric fields during the falling edge of the pulse accelerates again free electrons and/or induces field effects that lead to light emission. The amplitude of the H $\alpha$  emission quickly drops to very small values, although the electron densities decrease quite slowly. Apparently, the electron temperature for exciting the Balmer series drops much faster than the electron density. This is also typical for most afterglow plasmas.

Figure 9 shows the amplitude of the H $\alpha$  emission from the ionization region (same data as in figure 8) in comparison with the amplitudes of the H $\beta$  and H $\gamma$  emission from the recombination region. One can see that the amplitudes of lines from the ionization region and recombination region follow the same trend. One can also notice that the ratio between the H $\beta$  and H $\gamma$  amplitude drops as the plasma propagates. If one corrects the amplitudes for the different Einstein coefficients for these transitions, one may deduce a rather high population of the higher states, as being typical for recombination being the source of emission.

## 5. Discussion

The experiments yielded four major observations: (i) the electron density follows closely the same trend as the electrode voltage of the initial pulse. Correlating the peak in electron density to the maximum voltage, no time delay between ionization and voltage can be observed. (ii) Radiation from the ionization region is dominated by a Stark broadened H $\alpha$  emission from a very small region exhibiting high electron densities up to  $5 \times 10^{25} \text{ m}^{-3}$ ; (iii) radiation from the recombination region is dominated by H $\beta$  and H $\gamma$  emission. These lines are moderately broadened but are strongly affected by self absorption. The line ratios hint to recombination being the source of excitation; (iv) during the rising and the falling edge of the nanosecond pulse, emission goes through a maximum due to a variation of the governing electric fields. Based on these experimental observations, the following schematic picture of the plasma propagation inside the liquid is postulated and illustrated in figure 10:

- *Ignition by field ionization, figure 10(a):* at the onset of the voltage, a high electric field acts on the water layer adjacent to the electrode tip. The electric field strength is high enough at small protrusions to be able to induce field ionization of water molecules occurring above a threshold of the order of  $0.5 \text{ V \AA}^{-1}$ . The strong electric field surrounding these newly created positive water ions is high enough to even further ionize water molecules in the vicinity and a positive space charge region is starting to propagate through the liquid. This propagation should be dominated by field effects and may resemble hole conduction in solids, as it has already been postulated for the breakdown in transformer oils described by Zender theory for tunneling.
- *Formation of the plasma and initial electrode heating, figure 10(b):* due to the nonlinear interplay between electron transfer and local heating of the electrode, a localization of the electron current occurs and a particular spot on the tungsten tip reaches very high temperatures exceeding the boiling temperature of tungsten as a characteristic equilibrium temperature defined by the phase transition of tungsten. Thermionic emission of electrons may occur, although the electrons cannot easily escape the tungsten tip due to its positive voltage.

The time scale of plasma creation and propagation is governed by the time constant for ionization in competition with the time constant of recombination. Since the electron density in the ionization region follows closely the applied voltage and any delay between voltage and build-up of the electron density is not observed, it is reasonable to assume that the equilibrium between ionization and recombination is reached on a time scale much faster than the nanosecond scale of plasma propagation. This should correspond to the typical Saha equilibrium as a partial local thermal equilibrium PLTE. This is in contrast to the typical build-up of charges in a streamer in the gas phase at atmospheric pressure that takes usually 10 to 100 ns. In the case of the plasma propagation inside the



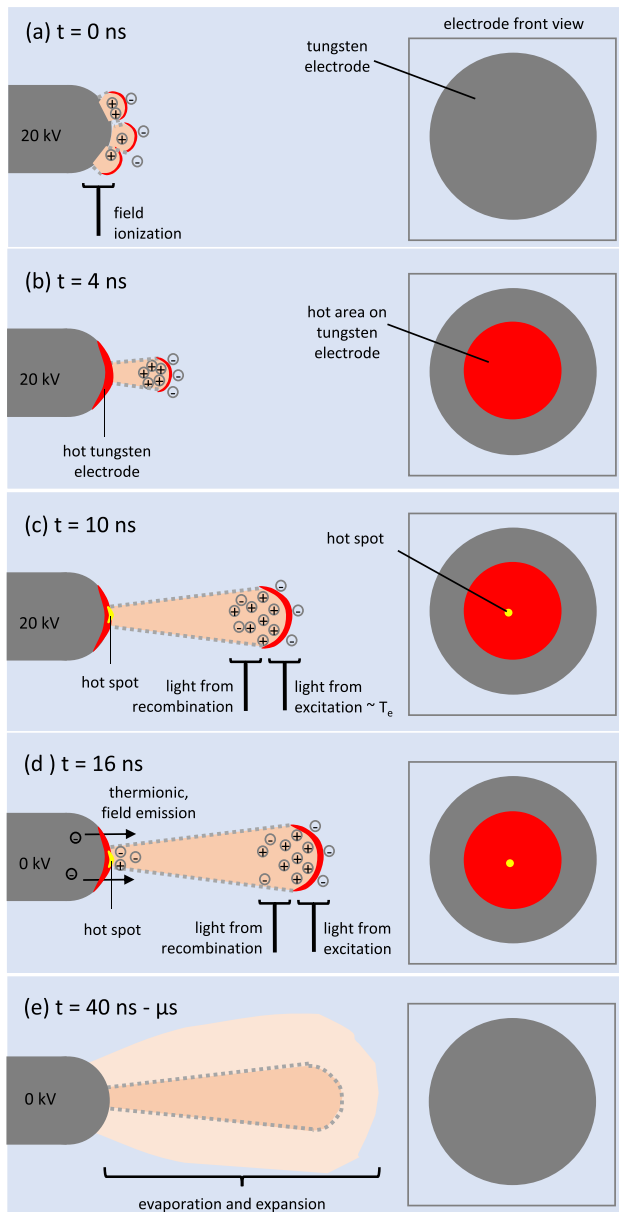


**Figure 10.** Sketch of plasma propagation in liquids: (a) field ionization of water molecules at the rising edge of the pulse, (b) hot spot formation and onset of plasma propagation, (c) plasma propagation, (d) end of the pulse, beginning of the falling edge of the pulse, (e) evaporation and expansion after the pulse. The right side of each sketch illustrates the front view onto the electrode tip and the grounded electrode is millimeters apart.

liquid, the density is a factor 1000 higher, implying much faster ionization with time constants of ps.

The ignition inside vapour bubbles in the tip vicinity that remain present from preceding discharges can be excluded. The residual vapour bubble after collapse separates from the electrode tip at 500  $\mu\text{s}$  after ignition before it moves upwards due to buoyancy [23]. The application of a voltage pulse with a frequency of 15 Hz creates a discharge every 67 ms which is much longer than the time for the vapour bubble to leave the tip vicinity. However, the presence of any nanovoids cannot be excluded from the experiments.

- **Plasma propagation**, figure 10(c): during the propagation of the plasma, new water molecules are ionized in the high electric field surrounding the positive space charge region. This process should exhibit a very local character being on the atomic scale: in the *gas phase*, a positive space charge propagates due to ionization events in the high electric field at the leading edge of the plasma. In the case of a classical positive streamer in gases, these ionization events consists of photo ionization that creates seed electrons ahead of the positive streamer head, that are accelerated into the streamer; in the *liquid phase* such a generation of seed electrons may occur similarly, but the strong recombination of any free electrons at far distances from the positive space charge region prevents any efficient acceleration. Therefore, new ionization events may occur either due to acceleration of free electrons along inter molecular distances in the liquid or by field effects at the boundary of the positive space charge. This distinction may be semantic and just demonstrates that a microscopic model of the propagation of the plasma is needed.

During propagation of the plasma, any ions that are left behind recombine on a short time scale. This implies a significant difference when comparing propagating plasmas in the gas and the liquid phase: in the *gas phase* a conductive and quasi neutral streamer channel is formed behind a positive streamer head; in the *liquid phase*, however, the formation of such a lasting conductive channel is unlikely, because recombination efficiently removes any charges on much shorter time scales than plasma propagation. Due to this, the structure of a propagating plasma in a liquid should correspond rather to an electric dipole propagating through the liquid consisting of a leading negatively charged edge followed by the small positive space charge region.

Light emission from the more positive part of the propagating dipole, should be dominated by recombination radiation originating from the region just behind the ionization region. This is consistent with the data, because the hydrogen Balmer emission labeled as originating from the recombination region is rather constant in time. In a classical streamer in the gas phase, the emission from the streamer channel would be expected to grow in time instead, because the length of a conductive channel in the gas phase is continuously increasing. This is not observed, and the light from the more positive recombination region follows a very similar temporal evolution as the light from the ionization region.

- **End of the pulse, field emission, plasma decay**, figure 10(d): at the end of the pulse, the electric fields decrease again. Then thermionic emission from the hot tungsten electrode, becomes possible leading to ionization and to a consecutive second maximum in emission at the falling edge of the high voltage pulse. During the decay of the voltage, the electron density follows closely the temporal evolution of the voltage.

- *Evaporation and expansion of the bubble/plasma channel, figure 10(e)*: on longer time scales from 10 ns to  $\mu$ s after plasma ignition, the water molecules and their dissociation products may start to move and evaporation and expansion of a bubble can occur. The heat of recombination along the propagating plasma channel may induce dissociative recombination, leading to excited OH molecules and H atoms. The recombination and relaxation of the species may lead to a thermal equilibrium of the species inside the plasma channel with a very high temperature and thus a very high pressure. Expansion and adiabatic cooling of the gas occurs, as it is already described in [23, 38].

This sequence of the dominating mechanisms during ignition, plasma propagation and decay describes consistently the temporal development of the emission data taken at very high temporal resolution. This description differs, however, from the classical description of streamer propagation in two main aspects: (i) first, recombination is much more important, so that the formation of a lasting conductive plasma channel as in gas discharges that lasts during the complete propagation of the plasma is unlikely, (ii) second, the ionization in the higher electric field region adjacent to the positive space charge should occur due to field effects rather than conventional acceleration of free electrons. Both effects require more detailed diagnostics in the future, but also more atomistic plasma models. Such models may exist in the field of laser produced plasmas, although ionization and propagation are very much dominated in those cases by the very intense laser field. Here, a plasma structure is only induced by an electric field in the very beginning.

Although the question of the discharge initiation mechanism remains difficult, we postulate that plasma generation and propagation may be dominated by field effects. This is supported by the fact that the electron density follows the same trend as the applied voltage. This similarity of the trends corroborates our hypothesis of the synchronization of the temporal axis of the voltage signal and the overall emission intensity. This indicates, that both ionization and recombination are happening very fast resulting from the  $10^3$  times higher species density in the liquid compared to gases. If the discharge would appear in gas filled microbubbles, this would result in a delay between voltage and electron density due to the build up of electron avalanches which take a few ns. Furthermore, if the excitation from a ground state gas density is assumed instead of liquid density, the same degree of self absorption which is calculated from the spectral lines would require  $10^3$  times larger plasma structures. This would result in propagating plasma heads of  $1000 \mu\text{m}$  and a streamer channel of 10 cm. This is not consistent with the ICCD images taken at the different times inside the plasma pulse. Furthermore, the open debate on favoring either ignition via electron impact ionization in nanovoids or field ionization inside the liquid has recently been elucidated by Aghdam and Farouk [40]. They implemented multi physics simulations of the ignition in a liquid due to nanosecond voltage pulses applied to a curved electrode and observed creation of low density regions due to electric field

induced pressure gradients and ionization by electron impact and field effects. Their main conclusion is that the threshold for cavitation is easily surpassed due to the short voltage rise times of the order of nanoseconds leading to low density regions with diameters of several microns at most and a density which is reduced only by a few percent compared to the liquid density. The electron impact ionization in these low density regions is too inefficient to explain plasma generation. Instead field ionization of water molecules has been identified as the main electron generation mechanism. This modeling insight into the microscopic nature of plasma ignition and propagation in a liquid is consistent with our interpretation of the data.

The propagation and development of that charged structure, however, occurs into the free space of a liquid at very high density and it remains an open question whether this propagation is similar to a streamer in the gas phase following a mechanism that is only properly scaled to the much higher densities or whether propagation is more likely governed by field effects and electron tunneling as in the models based on the Zener theory in semiconductors.

## 6. Conclusion

Nanosecond plasmas in liquids are analyzed by emission spectroscopy monitoring the temporal evolution of the hydrogen Balmer lines. Based on our experiments, we postulate that field effects are responsible for plasma ignition and plasma propagation. This is supported by two main observations: (i) the electrode voltage and plasma density follow the same trend. By correlating dark phase in intensity with the voltage plateau no phase delay between voltage and current can be observed as being typical for streamers in gases. The absence of a delay on the nanosecond scale between voltage and current supports thereby the hypothesis of plasma ignition and propagation directly inside the liquid which follows very fast time constants for ionization and recombination, so that the electron density is not a measure of the propagation of an avalanche but rather an equilibrium density from a balance between ionization and recombination; (ii) the optical depth causing self-absorption of the Balmer series is used to estimate the absolute species density of excited hydrogen atoms across the diameter of a streamer channel in the range of  $100 \mu\text{m}$ . This estimate yields only realistic values for typical electron temperatures, if we assume a density of H atoms in the ground state close to the liquid density of water molecules. The same optical depth assuming a ground state H atom density in the gas phase would imply a streamer channel diameter of 10 cm. This is not consistent with our experiment.

This assessment, however, is not necessarily a counter argument against ignition by electrostriction, since both effects, field ionization and electrostriction require similar field strengths and may occur at the same time and each contribution also may vary from experiment to experiment. Both effects require rather similar electric field strengths, so it is challenging to design an experiment to uniquely identify a particular mechanism. Two experimental options may exist: (i) if one succeeds to prepare two electrode tips with the same shape but different materials and thus different work function, the




effect of the electric fields could be separated from the electron tunnelling, because field effects depend on the work function. Such experiment requires a precise control of the shape of the electrode, independent on the choice of the material. This is challenging, because, as shown in part I of the paper series, the shape of the tip develops during plasma operation; (ii) the propagation of a gaseous streamer depends sensitively on the polarity distinguishing negative streamer propagating via an electron avalanche and positive streamer that require photon ionization as a mechanism to create the next electrons ahead of the streamer head. In case of field effects during plasma propagation, the difference between the appearance of negative and positive polarity should be small, because the direction of electron tunnelling either towards the anode or away of the anode follows the same tunnel barrier.

This illustrates that a decisive answer regarding the dominance of either effects, electrostriction or field effects require strong support from an atomistic modelling of plasma propagation in dense media. Such modelling should include quantum effects such as tunnelling, but also phase transitions of water.

## Acknowledgments

We would like to thank Julian Held for valuable discussions regarding spectroscopy and for the assistance on setting up the spectrometer. In addition, thanks are due to Behnaz Bagheri, Ute Ebert, and Satoshi Hamaguchi for general discussions on streamer physics. This project is supported by the DFG (German Science Foundation) within the framework of the Collaborative Research Centre SFB 1316 at Ruhr-University Bochum.

## ORCID iDs

A von Keudell  <https://orcid.org/0000-0003-3887-9359>  
K Grosse  <https://orcid.org/0000-0002-5770-9569>  
V Schulz-von der Gathen  <https://orcid.org/0000-0002-7182-3253>

## References

- [1] Foster J, Sommers B S, Gucker S N, Blankson I M and Adamovsky G 2012 *IEEE Trans. Plasma Sci.* **40** 1311–23
- [2] Jiang B, Zheng J, Qiu S, Wu M, Zhang Q, Yan Z and Xue Q 2014 *Chem. Eng. J.* **236** 348–68
- [3] Locke B R, Sato M, Sunka P, Hoffmann M R and Chang J S 2006 *Ind. Eng. Chem. Res.* **45** 882–905
- [4] Malik M A, Ghaffar A and Malik S A 2001 *Plasma Sources Sci. Technol.* **10** 82–91
- [5] Mizuno T, Ohmori T, Akimoto T and Takahashi A 2000 *Japan. J. Appl. Phys.* **39** 6055–61
- [6] Horikoshi S and Serpone N 2017 *RSC Adv.* **7** 47196–218
- [7] Geavlete B, Stanescu F, Iacoboaie C and Geavlete P 2013 *BJU Int.* **111** 793–803
- [8] Bruggeman P J et al 2016 *Plasma Sources Sci. Technol.* **25** 053002
- [9] Bruggeman P J and Leys C 2009 *J. Phys. D: Appl. Phys.* **42** 053001
- [10] Ceccato P, Guaitella O, Shaper L, Graham B and Rousseau A 2009 Time resolved imaging of a pulsed plasma discharge in water *IEEE Pulsed Power Conference* pp 866–71
- [11] Ceccato P H, Guaitella O, Le Gloahac M R and Rousseau A 2010 *J. Phys. D: Appl. Phys.* **43** 175202
- [12] Joshi R P, Kolb J F, Xiao S, Schoenbach K H and Schoenbach K H 2009 *Plasma Process. Polym.* **6** 763–77
- [13] Šimek M, Člupek M, Babický V, Lukeš P and Šunka P 2012 *Plasma Sources Sci. Technol.* **21** 055031
- [14] Dobrynin D, Seepersad Y, Pekker M, Shneider M, Fridman G and Fridman A A 2013 *J. Phys. D: Appl. Phys.* **46** 105201
- [15] Marinov I, Starikovskaia S and Rousseau A 2014 *J. Phys. D: Appl. Phys.* **47** 224017
- [16] Zhuang J, Sun A and Huo C 2016 *High Volt.* **1** 74–80
- [17] Šimek M, Pongráč B, Babický V, Člupek M and Lukeš P 2017 *Plasma Sources Sci. Technol.* **26** 07LT01
- [18] Pongráč B, Šimek M, Člupek M, Babický V and Lukeš P 2018 *J. Phys. D: Appl. Phys.* **51** 124001
- [19] Seepersad Y, Pekker M, Shneider M N, Fridman A A and Dobrynin D 2013 *J. Phys. D: Appl. Phys.* **46** 355201
- [20] Sharbaugh A, Devins J and Rzas S 1978 *IEEE Trans. Electr. Insul.* **EI-13** 249–76
- [21] Devins J C, Rzas S J and Schwabe R J 1981 *J. Appl. Phys.* **52** 4531–45
- [22] O'Sullivan F, Hwang J, Zahn M, Hjortstam O, Pettersson L, Liu Rongsheng and Biller P 2008 A model for the initiation and propagation of positive streamers in transformer oil *Conf. Record of the 2008 IEEE Int. Symp. on Electrical Insulation (Vancouver, BC: IEEE)* pp 210–4
- [23] Grosse K, Held J, Kai M and von Keudell A 2019 *Plasma Sources Sci. Technol.* **28** 085003
- [24] Grosse K, Schulz-von der Gathen V and von Keudell A 2020 *Plasma Sources Sci. Technol.* submitted
- [25] Ebert U and Sentman D D 2008 *J. Phys. D: Appl. Phys.* **41** 230301
- [26] Bagheri B et al 2018 *Plasma Sources Sci. Technol.* **27** 095002
- [27] Bergner A, Scharf F H, Kühn G, Ruhmann C, Hoebing T, Awakowicz P and Mentel J 2014 *Plasma Sources Sci. Technol.* **23** 054005
- [28] Gigoso M A, González M Á and Cardenoso V 2003 *Spectrochim. Acta, Part B* **58** 1489–504
- [29] van der Horst R M, Verreycken T, van Veldhuizen E M and Bruggeman P J 2012 *J. Phys. D: Appl. Phys.* **45** 345201
- [30] Konjević N, Ivković M and Sakan N 2012 *Spectrochim. Acta, Part B* **76** 16–26
- [31] Kielkopf J F and Allard N F 2014 *J. Phys. B: At. Mol. Opt. Phys.* **47** 155701
- [32] Konjević N 1999 *Phys. Rep.* **316** 339–401
- [33] Helbig V and Kusch H 1972 *Astron. Astrophys.* **20** 299
- [34] Cowan R D and Dieke G H 1948 *Rev. Mod. Phys.* **20** 418–55
- [35] Huddleston R and Stanley L 1965 *Plasma Diagnostic Techniques* 1st edn (New York: Academic)
- [36] Starikovskiy A, Yang Y, Cho Y I and Fridman A 2011 *Plasma Sources Sci. Technol.* **20** 024003
- [37] Simeni M S, Goldberg B, Gulko I, Frederickson K and Adamovich I V 2018 *J. Phys. D: Appl. Phys.* **51** 01LT01
- [38] Chauvet L, Nenbangkaeo C, Grosse K and Keudell A 2020 *Plasma Processes and Polymers*
- [39] An W, Baumung K and Bluhm H 2007 *J. Appl. Phys.* **101** 053302
- [40] Aghdam A C and Farouk T 2020 *Plasma Sources Sci. Technol.* **29** 025011